Journal of Luminescence 151 (2014) 123–129

Contents lists available at ScienceDirect

Journal of Luminescence

journal homepage: www.elsevier.com/locate/jlumin

# Spectroscopic characterization of $CaNb_2O_6$ single crystal doped with samarium ions

Adam Strzęp [a,*], Witold Ryba-Romanowski [a], Radosław Lisiecki [a], Xiaodong Xu [b], Jun Xu [b], Juqing Di [c]

[a] Institute of Low Temperature and Structure Research PAS, Okolna 2 str., 50-422 Wroclaw, Poland
[b] Key Laboratory of Transparent and Opto-functional Inorganic Materials, Shanghai Institute of Ceramics, Chinese Academy of Sciences, Shanghai 201800, China
[c] Key Laboratory of Materials for High Power Laser, Shanghai Institute of Optics and Fine Mechanics, Chinese Academy of Sciences, Shanghai 201800, China

ARTICLE INFO

*Article history:*
Received 11 November 2013
Received in revised form
5 February 2014
Accepted 8 February 2014
Available online 22 February 2014

*Keywords:*
Synchrotron radiation
Time resolved luminescence
Low temperature measurements
Judd–Ofelt analysis

ABSTRACT

Spectroscopic measurements of the calcium niobate $CaNb_2O_6$ single crystal doped with samarium ions were performed. Polarized absorption and emission spectra as well as luminescence decay curves of this material were recorded as a function of temperature in the 5–300 K temperature region. Analysis of low temperature spectra made it possible to determine energies of crystal field components of $Sm^{3+}$ multiplets involved in the excitation and luminescence phenomena. Number of crystal field levels derived implies that $Sm^{3+}$ ions in the $CaNb_2O_6$ host are accommodated in several different sites. Radiative lifetime of the $^4G_{5/2}$ metastable level determined based on the Judd–Ofelt analysis of room temperature absorption spectra amounts to 777 μs, a value close to that of luminescence lifetime determined from luminescence decay curve. Energy transfer between the $NbO_6$ group and samarium ions was observed in wide temperature range. Intense luminescence related to the $^4G_{5/2}\rightarrow{}^6H_{7/2}$ and $^4G_{5/2}\rightarrow{}^6H_{9/2}$ transitions centered at 610 nm and 660 nm, respectively, combined with strong absorption band near 404 nm that matches perfectly the pump light provided by commercial InGaN/GaN diode lasers points at a potential of $CaNb_2O_6$:$Sm^{3+}$ for the design of all-solid-state visible lasers.



## 1. Introduction

### 1.1. Motivation

Calcium niobate $CaNb_2O_6$ occurs in nature as a mineral Fermsite. It belongs to a group of Columbite ($FeNb_2O_6$) structure type minerals with general formula $AB_2O_6$ that crystallize in orthorombic crystal system in space group Pbcn ($D_{2h}^{14}$). $CaNb_2O_6$:RE (RE: Nd, Ho, Pr, Er, Tm, Yb) single crystals with high optical grade have been manufactured in the past and laser action in all of them has been reported [1,2]. $CaNb_2O_6$ could find potential application as active medium in Stimulated Raman Scattering lasers, due to strong $\chi^{(2)}$- and $\chi^{(3)}$- nonlinear activity [3,4]. Undoped $CaNb_2O_6$, when excited at 260 nm, exhibits luminescence in the form of a broad double band with maxima at 460 and 520 nm [5]. $CaNb_2O_6$ doped with $Ln^{3+}$ and codoped with $Ti^{4+}$ as a charge compensator has been proposed by Van der Voort et al. [6] as a low cost lamp phosphor. In recently published work the Czochralski growth and spectroscopic investigation of $CaNb_2O_6$:Sm crystal, including the Judd–Ofelt analysis of room temperature absorption spectra and evaluation of unpolarized room temperature emission spectra, have been reported [7]. In the present work we consider the effect of temperature on optical spectra and excited state relaxation dynamics of $Sm^{3+}$ ions and of the $NbO_6$ niobate group. Intention of this study is to get a more close insight into the nature of luminescent centers and to assess spectroscopic features relevant to a potential visible laser operation in the samarium doped $CaNb_2O_6$ crystal.

## 2. Experimental

A high optical quality $CaNb_2O_6$:Sm 2% at single crystal has been grown by the Czochralski method. Detailed information about sample preparation can be found in the paper by Di et al. [7]. The density of obtained crystal is 4.78 g/cm$^3$. Crystal axes were oriented exploiting the Laue method.

Optical measurements were carried out on a single crystal sample in the form of polished parallelepiped with dimensions $5.12\times5.00\times4.85$ mm$^3$ (cut perpendicular to crystallographic axes).

* Corresponding author. Tel.: +48 71 3954 182; fax: +48 71 344 1029.
*E-mail address:* a.strzep@int.pan.wroc.pl (A. Strzęp).

http://dx.doi.org/10.1016/j.jlumin.2014.02.018
0022-2313 

Spectral investigation was carried out in the 5–300 K temperature range.

Polarized absorption spectra were recorded using a Cary 5E Varian spectrophotometer. Spectral bandwidths were set to 0.2 nm and 1 nm for UV–vis and IR regions, respectively. Absorption spectra were measured in the range 300–2500 nm (33.330–4000 $cm^{-1}$).

Polarized emission spectra were measured using a DongWoo Optron DM750 monochromator coupled to a R-928 Hamamatsu photomultiplier. 150 W ozone free xenon lamp coupled to a DongWoo Optron DM151i monochromator was used as an excitation source.

Excitation spectra in a region of 150–330 nm and emission spectra excited in the above mentioned region were measured using the technical setup available at SUPERLUMI station at HASYLAB, DESY in Hamburg, Germany. Emission and excitation spectra acquired in HASYLAB were corrected for the spectral response of instruments and intensity of excitation source. Detailed information about this setup can be found in Ref. [8].

Coherent Libra femtosecond laser system coupled to a Light Conversion OPerA Optical Parametric Amplifier was used as an excitation source. Influence of femtosecond pulse on sample as well as luminescence decay curves was measured exploiting a Hamamatsu C5650 streak camera coupled to a Acton 2500i monochromator.

For low temperature measurements a continuous flow helium cryostat (Oxford model CF 1204) equipped with a temperature controller was used.

For polarized measurements Harrick PGT-S1V Glan-Taylor polarizers were used.

## 3. Results and discussion

### 3.1. Crystal structure considerations

Crystal structure of calcium niobate has been well established [9,1]. Cummings and Shimonsen report unit cell parameters of undoped crystal as $a=14.926$ Å, $b=5.752$ Å, and $c=5.204$ Å. Macalik et al. were investigating praseodymium doped calcium niobate and reported slightly different unit cell parameters $a=14.961$ Å, $b=5.740$ Å, and $c=5.217$ Å [10]. Crystal is composed of alternating calcium and niobium layers in *bc* crystallographic plane which are separated by oxygen anions. Comparison of ionic radius of $Sm^{3+}$ (1.10 Å), $Ca^{2+}$ (1.12 Å) and $Nb^{5+}$ (0.64 Å) leads to the conclusion that incorporated trivalent samarium ions should occupy preferentially $Ca^{2+}$ sites [11]. However, reports concerning location of lanthanide ions in sites different than supposed $Ca^{2+}$ sites can be found [10]. Most probably dissimilarity in sites is due to crystal lattice defects in coordination sphere of $Ln^{3+}$ induced by different charge of dopant ions (triply charged samarium ion substitutes doubly charged calcium). Local symmetry of $Ca^{2+}$ sites is $C_2$ (distorted cuboid) and coordination number is 8. Niobium ion is coordinated by six oxygen ions occupying apexes of distorted octahedron. One calcium cuboid adjoins with four other calcium cuboids and shares with them one edge per each. It also adjoins with eight niobium coordination polyhedra sharing edges with four of them and apexes with others. $NbO_6$ polyhedra adjoin six other niobium polyhedrons sharing edges with two of them, and apexes with others. Authors propose at least four different mechanisms of incorporation of samarium into lattice. Charge compensation could be fulfilled by the following factors:

1. creation of vacancy in $Ca^{2+}$ site, while two other neighboring $Ca^{2+}$ sites are occupied by $Sm^{3+}$ ions [$Ca^{2+}$–$Ca^{2+}$–$Ca^{2+}$ = $Sm^{3+}$–Vac–$Sm^{3+}$];
2. creation of vacancy in $O^{2-}$ site, while $Nb^{5+}$ site is occupied by $Sm^{3+}$ [$O^{2-}$–$Nb^{5+}$ = Vac–$Sm^{3+}$];
3. incorporation of additional oxygen ion between two $Sm^{3+}$ ions occupying adjoining $Ca^{2+}$ sites [$Ca^{2+}$–$O^{2-}$–$Ca^{2+}$ = $Sm^{3+}$–$O^{2-}$–$O^{2-}$–$Sm^{3+}$];
4. reduction of $Nb^{5+}$ to $Nb^{4+}$ when adjoining $Ca^{2+}$ site is occupied by $Sm^{3+}$ [$Ca^{2+}$–$O^{2-}$–$Nb^{5+}$ = $Sm^{3+}$–$O^{2-}$–$Nb^{4+}$].

The last point should be discussed more carefully. After reduction electron configuration of niobium ion will be [Kr]$4d^1$; thus it should

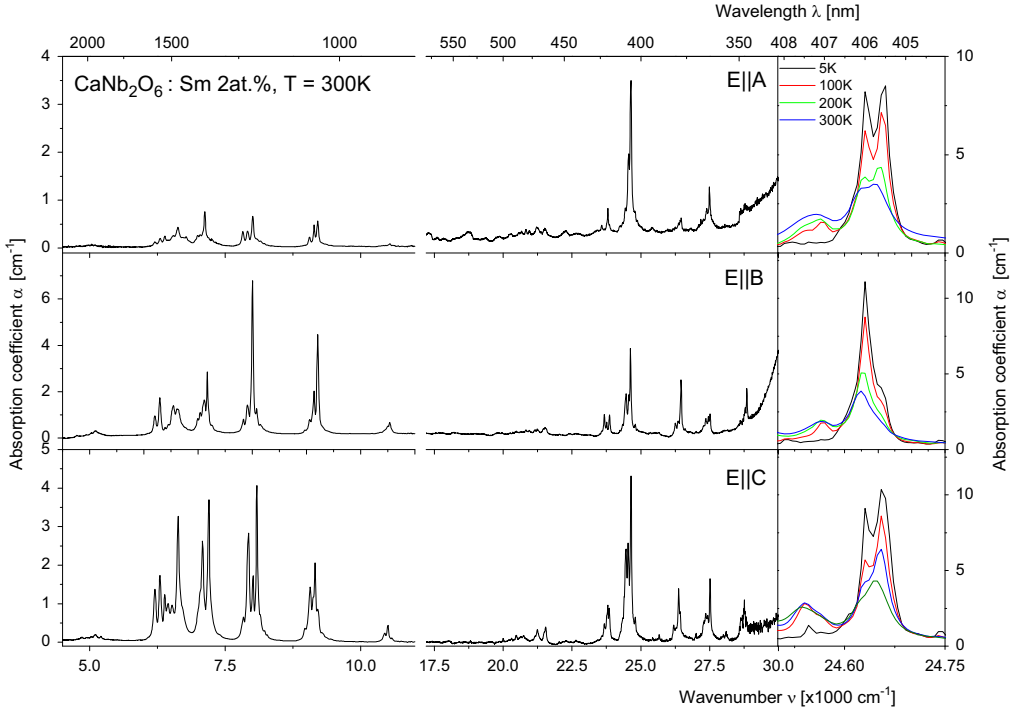


**Fig. 1.** Polarized room temperature absorption spectra of $CaNb_2O_6$:$Sm^{3+}$ 2 at% crystal. On the right side influence of temperature on shape and intensity of most prominent band in visible part of spectrum is shown.

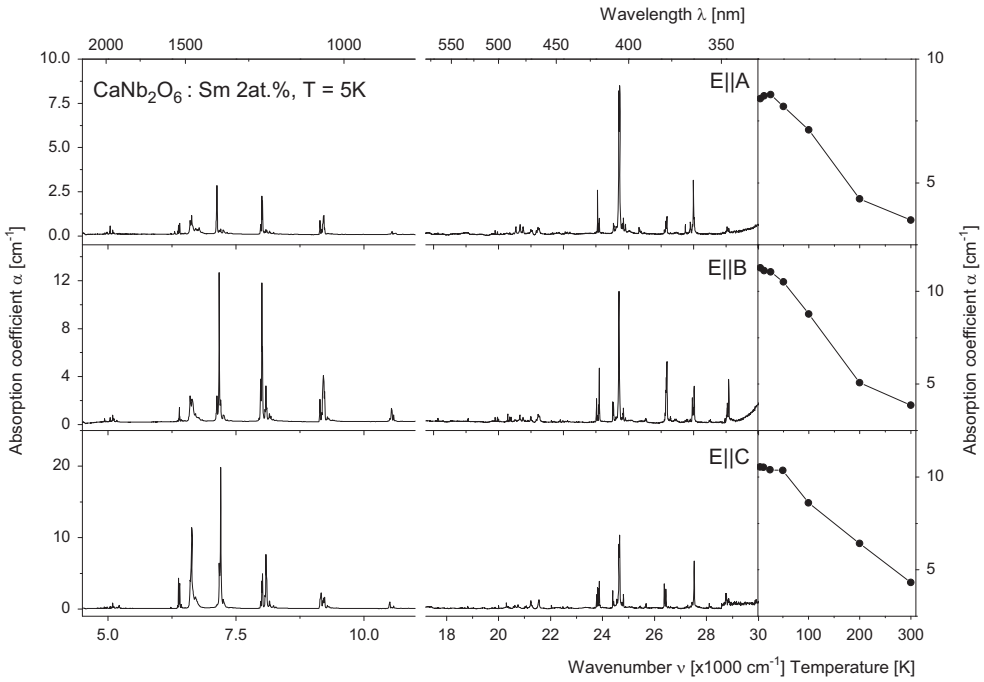


**Fig. 2.** Polarized absorption spectra of $CaNb_2O_6$:$Sm^{3+}$ 2 at% collected at $T=5$ K. On the right side influence of temperature on peak absorption coefficient for transition ca. 406 nm is shown.

become optically active. This should be reflected in occurrence of additional broad and intense absorption bands. However, undoped matrix as same as Sm doped $CaNb_2O_6$ does not show any broad and intense absorption bands in 400–2000 nm range. Accordingly the latter mechanism is not corroborated by experimental data.

### 3.2. Absorption spectra

All materials that crystallize in the orthorhombic, monoclinic, or triclinic crystal systems are optically biaxial. In orthorombic crystals optical indicatrices are colinear with crystallographic axes. To get knowledge about optical properties of crystal investigated, polarized absorption spectra in temperature range 5–300 K were recorded. Absorption spectra collected at room temperature and at 5 K, shown in Figs. 1 and 2 respectively, reveal strong influence of crystal anisotropy on absorption bands. Strong influence of incident light polarization on transitions intensities was also observed in Pr or Tm doped $CaNb_2O_6$ [10,12].

On the right side of Fig. 1 the effect of temperature on shape and intensity of the most intense absorption band located at ca. 406 nm in the UV–vis part of spectrum is shown. On the right part of Fig. 2 the influence of temperature on absorption coefficient at the band maximum is presented. High intensity combined with relatively large spectral width of 1.5 nm (FWHM) is favorable for optical pumping by commercially available GaN/InGaN laser diodes. With decreasing temperature the band divides into two lines centered at 406 and 405.5 nm for E||*a* and E||*c* polarizations, respectively while for E||*b* polarization the line at 406 nm occurs, which is shown on the right side of Fig. 1. Nevertheless, for all polarizations the width of this band is almost independent of temperature. As a consequence, the spectral overlap between a pump emission spectrum and absorption band will be independent of temperature, too. As can be seen in Fig. 2, the peak value of absorption coefficient increases more than 2 times, when temperature drops from 300 K to 100 K. Polarizations E||*b* and E||*c* shows higher absorption coefficients, thus optical pumping along with crystallographic *a* axis should be favorable. In addition to $Sm^{3+}$ bands a steep absorption related to transitions within electronic structure of $NbO_6$ group [5] below ca. 350 nm contributes to the $CaNb_2O_6$:Sm absorption spectrum. This band, as can be seen in Figs. 1 and 2, is also polarization sensitive.

Energies of Stark levels for selected multiplets of $Sm^{3+}$ ions have been derived from low temperature spectra and are gathered in Table 1.

As one can see, bands related to transitions from ground state to $^6F_{1/2}$, $^6F_{5/2}$, $^6F_{7/2}$, and $^6F_{9/2}$ possess more lines that emerge from their Stark splitting. Occurrence of additional lines could emerge from two reasons: (*I*) presence of more than one crystal environment for samarium ions, or (*II*) small energy difference between lowest Stark components of ground level. It is easy to discern which phenomenon is responsible for occurrence of additional lines. If ground state possesses Stark components that differ slightly in energy, absorption spectra should differ a lot in different temperatures. From collected data one can see that energy difference between first two Stark components is around 20 $cm^{-1}$. According to Boltzmann equation upper level should be populated in 1% in 6.25 K and in 10% in 12.5 K. This increase of population should reflect in ten times intensity increase of line related to transition from second Stark level of ground state to the lowest Stark component of excited state. Above described situation does not occur; thus occurrence of additional lines can be explained only by multiplicity of environments around samarium ions. Reasons of this phenomena have been explained in Section 3.1. Various defects affect crystal field in different way; thus samarium ions located in different crystal environments possess distinct splitting of Stark levels. These defects lead to an inhomogeneous broadening of absorption and emission bands. Broad absorption bands are favorable for the purpose of optical pumping. On the other hand broad emission bands offer a possibility to obtain broader emission gain bandwidths, or shorter pulse duration, if a mode locked laser operation is considered.

### 3.3. Calculations in frame of the Judd–Ofelt phenomenological model

#### 3.3.1. Short introduction to Judd–Ofelt theory

Radiative transitions within electronic $4f^n$ sub-shell of lanthanide ions are mainly governed by two mechanisms: electric dipole

**Table 1**
Stark levels of selected multiplets. Assignment to multiplets was done using values of $\|U^T\|U^t$ parameters taken from [13].

| Mult. | Energy of Stark levels ($cm^{-1}$) | Exp/ther | $\Delta E$ |
|---|---|---|---|
| $^6F_{1/2}$ | 6377, 6392, 6400 | 3/1 | 23 |
| $^6F_{3/2,}$ $^6H_{15/2}$ | 6602, 6618, 6633, 6648, 6711, 6779 | – | – |
| $^6F_{5/2}$ | 7110, 7128, 7174, 7199, 7249, 7265 | 6/3 | 155 |
| $^6F_{7/2}$ | 7971, 7981, 8006, 8019, 8039, 8068, 8084, 8100, 8153, 8183 | 10/4 | 212 |
| $^6F_{9/2}$ | 9144, 9162, 9174, 9195, 9212, 9229, 9285, 9306, 9324 | 9/5 | 180 |
| $^6F_{11/2}$ | 10,509, 10,537, 10,548, 10,576 | 4/6 | 67 |
| $^4G(4)_{5/2}$ | 17,671 | 1/3 | - |
| $^4F(3)_{3/2}$ | 18,808, 18,829 | 2/2 | 21 |
| $^4G(4)_{7/2}$ | 19,869, 19,928, 19,956, 20,000 | 4/4 | 131 |
| $^4M_{15/2}$, $^4I(3)_{11/2}$, $^4I(3)_{13/2}$, $^4F(3)_{5/2}$ $^4M_{17/2}$, $^4G(4)_{9/2}$, | 20,300, 20,354, 20,429, 20,483, 20,627, 20,820, 20,942, 21,021, 21,128, 21,245, 21,450, 21,519, 21,565, 22,031, 22,134, 22,336, 22,376, 22,477, 22,563, 22,650, 22,722 | – | – |
| $^6P_{3/2}$ | 23,770, 23,787, 23,849, 23,872 | 4/2 | 102 |
| $^6P_{5/2}$ | 24,390, 24,420, 24,630, 24,661, 24,783, 24,801, 24,882 | 7/3 | 492 |
| $^6P_{7/2,}$ $^4L_{17/2,}$ $^4K(1)_{13/2}$ | 26,378, 26,413, 26,455, 26,476 | – | – |
| $^4D(2)_{3/2,}$ $^6P_{5/2}$ | 27,375, 27,450, 27,495, 27,525 | – | – |
| $^6P_{7/2}$ | 28,801, 28,852 | 2/4 | 51 |

and magnetic dipole. Oscillator strength of radiative transition is thus a sum of magnetic and electric dipole oscillator strengths which can be expressed as

$$f_{osc} = f_{md} + f_{ed} \tag{1}$$

A phenomenological model developed separately by Judd and Ofelt [14,15] allows us to predict oscillator strengths for electric dipole transitions. According to this model a parameter called line strength for transition between initial $|aJ>$ and final $|bJ'>$ states depends on three $\Omega_T$ parameters. The relation could be expressed as

$$S_{ed} = \sum_{T=2,4,6} \Omega_T \cdot \langle aJ||U^T||bJ'\rangle^2 \tag{2}$$

where $\Omega_T$ are three spectroscopic parameters and $\langle aJ\|U^T\|bJ'\rangle^2$ are the squares of double reduced matrix elements of unit tensor operator $\|U^T\|$ which connects $|aJ>$ and $|bJ'>$ states. Oscillator strengths are related to line strength according to the following formula:

$$f_{ed} = \frac{8\pi^2 cm\nu}{3h(2J+1)} \cdot \chi_{ed} \cdot S_{ed} \tag{3}$$

where $\nu$ denotes the wavenumber related to $|aJ> \rightarrow |bJ'>$ transition, $h$ is the Planck constant and $\chi$ is the Lorentz local field correction factor expressed as

$$\chi_{ab} = \frac{(n^2+2)^2}{9n}, \quad \chi_{emi} = \frac{n(n^2+2)^2}{9} \tag{4}$$

for absorption and emission measurements respectively.

The $\Omega_T$ parameters are calculated by application of a least squares fitting method to the set of above mentioned equations where values of oscillator strengths of appropriate transitions are calculated by numerical integration of absorption bands according to the following formula:

$$f_{osc}\langle aJ\left|bJ'\right\rangle = \frac{mc}{me^2N}\int \alpha(\nu)\partial\nu \tag{5}$$

where $N$ means the density of dopant ions evaluated to be $2.524 \times 10^{20}$ [ions/cm$^3$], $m$, $e$ and $c$ are the electron mass, electron charge and the velocity of light, respectively. $\alpha(\upsilon)$ is the absorption coefficient. The $\|U^T\|^2$ parameters are in principle host invariant; thus for our calculation we used values reported in Ref. [13]. Value of $f_{md}$ is usually negligible contrary to $f_{ed}$. However it can be easily calculated knowing its value in different material and refractive indexes of investigated and reference materials according to the following formula:

$$\chi_{md} \cdot S_{md} = \chi'_{md} \cdot S'_{md} \tag{6}$$

where $S_{md}$ is magnetic dipole line strength of transition and $\chi_{md}$ is Lorentz factor equal:

$$\chi_{ab} = n, \quad \chi_{emi} = n^3 \tag{7}$$

for absorption and emission measurements respectively (prime signs denote reference data).

When $\Omega_T$ parameters are known, some emission characteristics of material governed by electric dipole transition can be calculated. Those parameters are (*I*) radiative transition probabilities A, (*II*) branching ratios $\beta$ and (*III*) radiative lifetime $\tau_{rad}$ of metastable levels for which following formulas apply:

$$(I): \quad A\langle aJ|bJ'\rangle = \frac{64\pi^4\nu^3}{3h(2J+1)} \cdot (\chi_{ed} \cdot S_{ed} + \chi_{md} \cdot S_{md}) \tag{8}$$

$$(II): \quad \beta = \frac{A\langle aJ|bJ'\rangle}{\sum A\langle aJ|bJ'\rangle} \tag{9}$$

$$(III): \quad \tau_{rad} = \frac{1}{\sum A\langle aJ|bJ'\rangle} \tag{10}$$

where summation always occur to all multiples possessing lower energy.

### 3.3.2. Discussion on obtained results

Examination of polarized absorption spectra shown in Fig. 1 reveals that they differ markedly for one polarization from those reported in [7]. In the cited work mistake was made during preparation of absorption spectra figure (polarizations $E\|a$ and $E\|b$ in Fig. 4 from Ref. [7] looks the same, while Judd–Ofelt intensity parameters gathered in Table 3 therein differs strongly). Analysis of absorption spectra was performed in the framework of the Judd–Ofelt phenomenological model [14,15]. The $4f^5$ electronic configuration of $Sm^{3+}$ ion is split into 198 $^{2S+1}L_J$ multiplets which are divided into 2002/2 $^{2S+1}L_J(M_J)$ Krammer's doublets. Excited multiplets located above 18,000 $cm^{-1}$ are so closely spaced that energy difference between them is comparable to their Stark splitting. As a consequence the assignment of absorption bands in the visible and UV region is difficult. For example, the most intense absorption band at ca. 406 nm may be related, in principle, to transitions ending on the $^4M_{19/2,}$ $^4L_{13/2}$, $^4P_{5/2}$, $^4F_{7/2}$ and $^6P_{5/2}$ excited multiplets. Overall oscillator strength of a band is given by

the sum of electric and magnetic dipole oscillator strengths of all transitions involved. Value of electric dipole strength for each transition is proportional to a sum of products of intensity parameters $\Omega_t$ and squared doubly reduced matrix elements $\|U^T\|^2$.

$$f_{ed} \sim \sum_{T=2,4,6} \Omega_T \cdot \langle aJ||U^T||bJ'\rangle^2 \quad (11)$$

Values of $\|U^T\|^2$ change only slightly depending on the host. Examination of $\|U^T\|^2$ matrix elements makes it possible to neglect the contribution of transitions characterized by matrix elements equal or close to zero. In fact, it follows from $\|U^T\|^2$ matrix elements tabulated in [13] that the intensity of the band mentioned above is essentially due to the $^6H_{5/2}$–$^6P_{5/2}$ transition.

The polarized absorption spectra at 300 K were used to calculate the oscillator strengths for different polarizations. Intensities of transition in $CaNb_2O_6$:Sm crystal were evaluated by means of numerical integration of absorption bands. Calculated oscillator strengths as well as spectroscopic $\Omega_T$ parameters are collected in Table 2. In Table 3 a comparison of obtained parameters with other matrices is shown. From all materials compared calcium niobate possesses the highest $\Omega_2$ and almost highest $\Omega_4$ parameters. When comparing $\|U^T\|^2$ parameters for transitions originating from $^4G_{5/2}$ to multiplets of terms $^6H$ and $^6F$ one can see that relatively high values of $\|U^2\|^2$ can be found only for transitions to $^6F_J$ ($J=5/2$, 7/2) while $\|U^4\|^2$ for transitions to $^6H_J$ ($J=7/2$, 9/2) are very small [13]. By appropriate selection of matrix it is possible to obtain materials emitting more light in orange-red or infrared part of spectrum. In investigated material both $\Omega_2$ and $\Omega_4$ parameters are high; thus oscillator strengths for above mentioned multiplets are significant. High values of $\Omega_T$ parameters are also reflected in short lifetime of metastable level. But short lifetime has positive influence on emission cross section, which is an important parameter concerning laser operation. Based on obtained intensity parameters $\Omega_t$ transition probabilities $A$, luminescence branching ratios $\beta_R$, and radiative lifetime $\tau_r$ were calculated. Results are gathered in Table 4. Obtained intensity parameters differ from those shown in the work in Ref. [7], what emerges from different ways of calculating them. In the work in Ref. [7] intensity parameters ($\Omega^T$) were calculated separately for each polarization, and after that mean value was obtained. In this work calculation of intensity parameters was done in a different way. Firstly mean value of oscillator strength for specific transition in different polarizations was calculated. Set of obtained mean oscillator strengths was taken for calculation of Judd–Ofelt intensity parameters. This procedure seems to be more appropriate contrary to previous one, what is well explained in Ref. [16].

**Table 2**
Experimental and calculated oscillator strengths for transitions within $4f^5$ configuration of $Sm^{3+}$ ion in $CaNb_2O_6$. Spectroscopic parameters $\Omega_T$ were calculated using $U^T$ parameters taken from Ref. [13]. For calculations only $^6H_{5/2}$ to $^6H_{13/2,\ 15/2}$ and $^6F_J$ transitions were used.

| Transition from $^6H_{5/2}$ to | Energy ($cm^{-1}$) | Oscillator strength ($\times 10^{-6}$) | | | | | Residual |
|---|---|---|---|---|---|---|---|
| | | $P_a$ | $P_b$ | $P_c$ | $P_{mean}$ | $P_{calc}$ | |
| $^6H_{13/2}$ | 5038 | 0.59 | 1.25 | 1.35 | 1.06 | 0.98 | 0.08 |
| $^6F_{3/2,}$ $^6H_{15/2,}$ $^6F_{5/2}$ | 7123 | 9.21 | 30.16 | 46.59 | 28.65 | 28.7 | 0.05 |
| $^6F_{7/2}$ | 8006 | 4.03 | 19.65 | 20.57 | 14.75 | 14.7 | 0.05 |
| $^6F_{9/2}$ | 9208 | 2.86 | 14.75 | 11.75 | 9.79 | 9.8 | 0.01 |
| $^6F_{11/2}$ | 10,537 | 0.36 | 2.22 | 1.63 | 1.40 | 1.6 | 0.2 |

Spectroscopic parameters $\Omega_2=8.02\pm0.35$, $\Omega_4=5.37\pm0.31$, $\Omega_6=3.74\pm0.08$ [$\times 10^{-20}$ $cm^2$].

**Table 3**
Comparison of spectroscopic $\Omega_T$ parameters for various compounds doped with samarium ions.

| Material | | $\Omega_2$ | $\Omega_4$ | $\Omega_6$ | $\tau_{rad}$ | Ref. |
|---|---|---|---|---|---|---|
| Glasses | 40 $Li_2O$–4 $Nb_2O_5$–55 $B_2O_3$–1 $Sm_2O_3$ | 5.13 | 4.91 | 4.03 | 2205 | [17] |
| | 55 $P_2O_5$–39 PbO–5 $Nb_2O_5$–1 $Sm_2O_3$ | 1.72 | 3.42 | 2.80 | 2820 | [18] |
| Crystals | $CaNb_2O_6$ | 8.02 | 5.37 | 3.74 | 777 | This |
| | $LiNbO_3$ | 2.11 | 4.50 | 1.45 | 1122 | [19] |
| | α-$Na_3Y(VO_4)_2$:Sm | 2.50 | 1.54 | 0.76 | 3408 | [20] |
| | $LiYF_4$ | 0.55 | 2.44 | 1.72 | 6900 | [21] |
| | $K_2YF_5$ | 0.38 | 3.55 | 2.18 | 5180 | [22] |
| | $K_5Li_2LaF_{10}$ | 4.30 | 3.60 | 1.84 | 6950 | [23] |
| | $Gd_2SiO_5$ | 1.12 | 5.57 | 2.78 | 1800 | [24] |
| | $(Lu_{0.4}Gd_{0.6})_2SiO_5$ | 1.26 | 4.68 | 2.32 | 1800 | [25] |

### 3.4. Emission and excitation characteristics

Polarized emission spectra, when excited into $^6H_{5/2}\rightarrow{}^6P_{3/2}$ transitions of $Sm^{3+}$ ion, collected at room temperature are shown in Fig. 3(a)–(c). Spectral bandwidth of monochromator was set to 0.1 nm, but obtained data are not corrected for spectral response of system used. Fig. 3(d) shows an unpolarized emission spectrum recorded employing a low resolution monochromator coupled with a ccd detector, which is corrected for spectral response of recording system. Large spectral widths of luminescence bands result from location of $Sm^{3+}$ ions in different disordered coordination sites. Charge mismatch between $Ca^{2+}$ and $Sm^{3+}$ affect concentration of defects in crystal lattice, what also leads to broadening of bands. At room temperature 7 components can be distinguished for the $^4G_{5/2}\rightarrow{}^6H_{7/2}$ band centered at 610 nm. Two overlapping lines centered at 608.5 and 610 nm dominate this band. FWHM parameter for this conjugated lines is 3.2 nm.

Widths of lines diminish fast with decreasing temperature. It can be seen in Fig. 4 that already at 100 K emission spectra consist of well separated lines related to transitions between individual crystal field levels. Fig. 4 shows effect of temperature on polarized emission bands calibrated in units of emission cross sections $\sigma_{em}$ that were calculated based on Fuchtbauer–Ladenburg equation:

$$\sigma_{em} = \frac{\beta\lambda^4}{8\pi c\tau_{rad}n^2}\cdot\frac{I_{em}}{\int(I_{em}x+I_{em}yd\lambda I_{em}z)} \quad (12)$$

where $\beta$ is a branching ratio equal to 0.37 for $^4G_{5/2}\rightarrow{}^6H_{7/2}$ and 0.42 for $^4G_{5/2}\rightarrow{}^6H_{9/2}$ transitions. Velocity of light, wavelength, radiative lifetime and refractive index are denoted as $c$, $\lambda$, $\tau$ and $n$, respectively. Values of last two parameters are equal to 0.8 ms and 2.20 respectively. As can be seen in Fig. 4 the $\sigma_{em}$ maxima for five wavelengths at 5 K are advantageously high. These strong lines occur at 16,611 ($E\|b$), 16,445 ($E\|a$, $c$), 16,393 ($E\|a$, $b$, $c$), 15,244 ($E\|a$, $c$) and 15,193 [$cm^{-1}$] ($E\|a$, $b$, $c$). The highest value of $\sigma_{em}$ equal to $3.07\times10^{-21}$ $cm^2$ can be found at 15,244 $cm^{-1}$ for $E\|c$ polarization. This suggest possibility of obtaining laser action at 5 different wavelengths at liquid helium temperature. Values of $\sigma_{em}$ drops only slightly when temperature is raised from liquid helium to 100 K. The decrease in $\sigma_{em}$ values is slower for transitions terminating in $^6H_{7/2}$ multiplet than in $^6H_{9/2}$ one, pointing at a possibility to obtain laser action at two different wavelengths in the orange part of spectrum instead of red one.

Emission spectra excited at 260 nm and recorded at 300 K and 5 K are shown in Fig. 5(a) and (b), respectively. Broad band centered at ca. 490 nm can be assigned to relaxation of excited niobate group. In fact, when excited at 260 nm an undoped $CaNb_2O_6$ exhibits strong blue luminescence related to transitions within electronic structure of $NbO_6$ group. Niobate groups with oxygen vacancies are considered to be responsible for luminescence band centered at ca. 520 nm [5]. Incorporation of $Sm^{3+}$ ions

**Table 4**
Radiative transitions probabilities ($A_{ed}$ and $A_{md}$), radiative lifetime ($\tau_R$) and branching ratios ($\beta_{Teor}$ and $\beta_{Exp}$) for excited level $^4G_{5/2}$ of $Sm^{3+}$ in $CaNb_2O_6$ crystal. Magnetic dipole transition probabilities were recalculated from corresponding values given in [26].

| S'L'J' | $A_{ed}$ ($s^{-1}$) | $A_{md}$ ($s^{-1}$) | $A$ ($s^{-1}$) | $\beta_{Teor}$ | $\beta_{Exp}$ |
|---|---|---|---|---|---|
| $^6H_{5/2}$ | 34.6 | 20.8 | 55.4 | 4.30 | 7.32 |
| $^6H_{7/2}$ | 409.2 | 17.3 | 426.5 | 33.12 | 37.06 |
| $^6H_{9/2}$ | 536.7 | 0.0 | 536.7 | 41.68 | 42.86 |
| $^6H_{11/2}$ | 101.1 | 0.0 | 101.1 | 7.85 | 6.06 |
| $^6H_{13/2}$ | 18.1 | 0.0 | 18.1 | 1.40 | 0.57 |
| $^6F_{1/2}$ | 12.8 | 0.0 | 12.8 | 0.99 | |
| $^6H_{15/2}$ | 1.1 | 0.0 | 1.1 | 0.09 | 6.13 |
| $^6F_{3/2}$ | 13.9 | 7.2 | 21.2 | 1.64 | |
| $^6F_{5/2}$ | 85.7 | 4.9 | 90.6 | 7.04 | |
| $^6F_{7/2}$ | 9.8 | 1.5 | 11.4 | 0.88 | – |
| $^6F_{9/2}$ | 11.9 | 0.0 | 11.9 | 0.92 | – |
| $^6F_{11/2}$ | 0.9 | 0.0 | 0.9 | 0.07 | – |

$\Sigma_A = 1287.7$, $\tau_R = 777\ \mu s = 0.78$ ms.

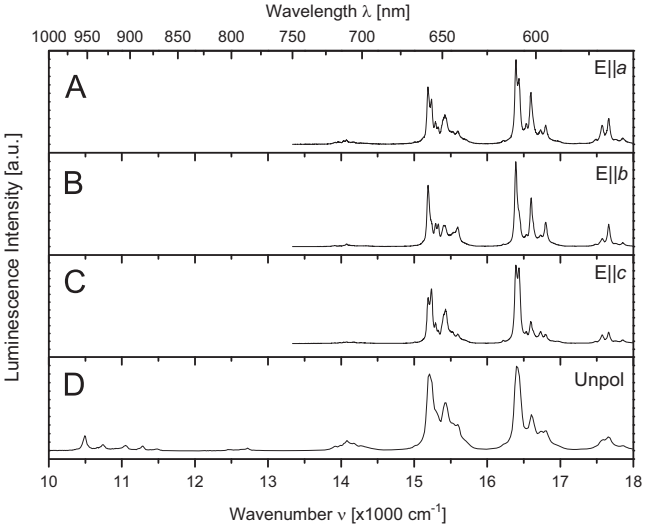


**Fig. 3.** Room temperature emission spectra of $CaNb_2O_6$:$Sm^{3+}$ 2 at%. Sample was excited into $^6H_{5/2}$ $^6P_{3/2}$ transition of $Sm^{3+}$ at ca. 406 nm. Polarized spectra were recorded exploiting a high resolution monochromator, but are not corrected for spectral response of the measurement system. Unpolarized spectrum was recorded on a CCD detector coupled with a low resolution monochromator, but this spectrum is corrected for spectral response.

results in new emission bands in orange–red part of spectrum. Depending on excitation wavelength, the $CaNb_2O_6$:Sm system can emit white or orange light. Appropriate mixture of blue–green luminescence from niobate groups with orange–red luminescence from samarium ions could lead to emission of white light. This feature of investigated material may be used in the construction of commercial phosphors for luminescent lamps.

Excitation spectra of luminescence in both the niobate group and $Sm^{3+}$ ions collected at room temperature are shown in Fig. 5 (c). Occurence of a strong band, spreading from 200 to 290 nm, when $^4G_{5/2} \rightarrow {}^6H_{7/2}$ transition was monitored, is an evidence of energy transfer from $NbO_6$ group to $Sm^{3+}$ ions. Examination of shape of excitation bands reveals that the maximum for the 610 nm band is shifted to higher $\lambda$ values in comparison to the excitation of 480 nm emission. This shift suggests that more than one kind of niobate groups (e.g. defected) take part in the energy transfer process. Exploiting synchrotron radiation made it possible to investigate excitation spectrum up to 150 nm; however no other excitation bands have been revealed in the investigated region.

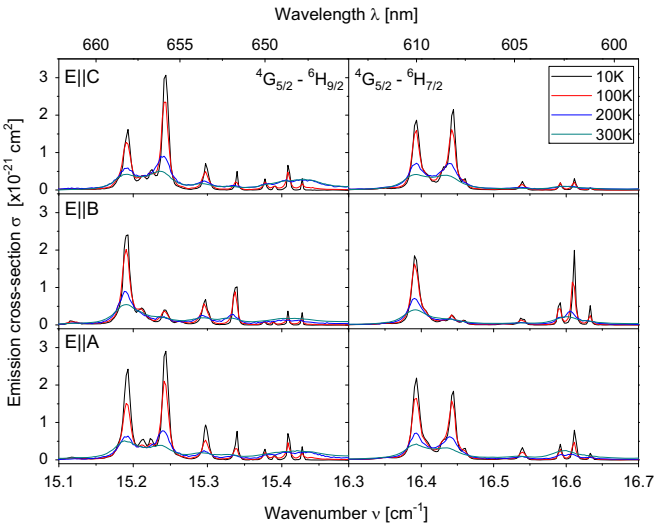


**Fig. 4.** Emission cross-sections for three polarizations collected at different temperatures.

### 3.5. Relaxation characteristics of luminescent levels

Visible luminescence of the system under study originates from two different active centers. First, there is the $NbO_6$ niobate group that emits in a broad spectral range spreading from 400 to 600 nm. Second, there are $Sm^{3+}$ ions that emit mainly in three bands centered at ca. 575, 610 and 660 nm respectively. Relaxation kinetics of both types of luminescence centers were investigated in the 10–300 K temperature range and results are shown in Fig. 6. In the whole temperature range obtained decay curves exhibit single exponential behavior. For niobate group the maximum of band at ca. 480 nm was monitored, and 260 nm line generated by OPA was used as an excitation source. For $Sm^{3+}$ a 610 nm line of the $^4G_{5/2}$– $^6H_{7/2}$ transition was monitored, and 406 nm line generated by OPA was used as an excitation source. It was found that the lifetime of samarium emission is almost independent of temperature (within observed temperature range), and in 300 K is equal to 730 μs. This value is close to one predicted in the framework of the Judd–Ofelt model (777 $\mu s$) what leads to ca. 94% quantum efficiency. On the other hand the lifetime of emission from the niobate group decreases markedly with increasing temperature. Such a behavior of lifetimes of the niobate group is consistent with data presented by Buth and Blasse [5]. Decreasing value of lifetime of niobate group with increasing temperature results from strong coupling of this transition with lattice vibrations (vibronic transition). In the case of samarium, transition is purely electronic in nature and due to high energy difference between states involved in transition coupling with lattice vibrations is negligible; thus lifetime of $^4G_{5/2}$ level is independent of temperature.

## 4. Conclusions

Spectroscopic properties of Sm ions in $CaNb_2O_6$ single crystal are reported. Taking into account ionic radii of cations present in the host lattice one may suppose that samarium ions should preferentially enter well defined calcium sites with $C_2$ symmetry. However, low temperature spectra reveal more lines than expected implying that samarium ions are located in different crystal environments. Energy transfer between the niobate group and samarium ions has been observed in wide temperature range. Mixture of emission in blue–green region from niobate groups and orange–red

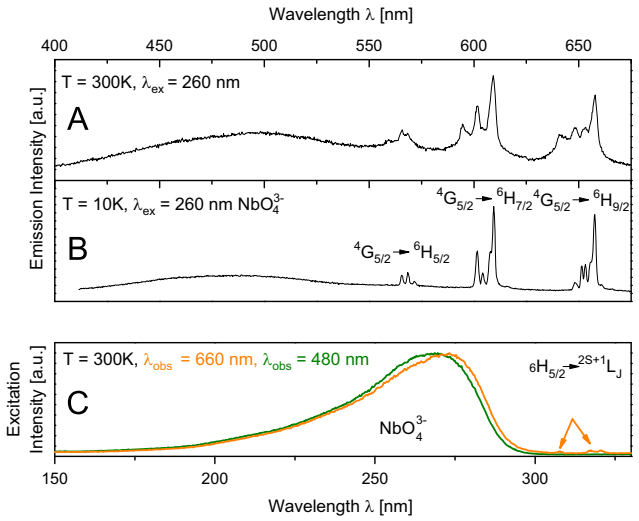


**Fig. 5.** Effect of temperature on unpolarized emission spectra, when sample was excited into band related to transition within electronic structure of niobate group. Three lines at ca. 575, 610 and 650 nm are related to transitions from $^4G_{5/2}$ multiplet of $Sm^{3+}$ ions. Occurrence of these lines in these spectra is an evidence of energy from niobate group to samarium ions. In the lower part excitation spectra of $CaNb_2O_6$:$Sm^{3+}$ 2 at% collected at room temperature are shown. Weak lines in upper spectrum can be assigned to intracofigurational transitions within 4f shell of $Sm^{3+}$ ion.

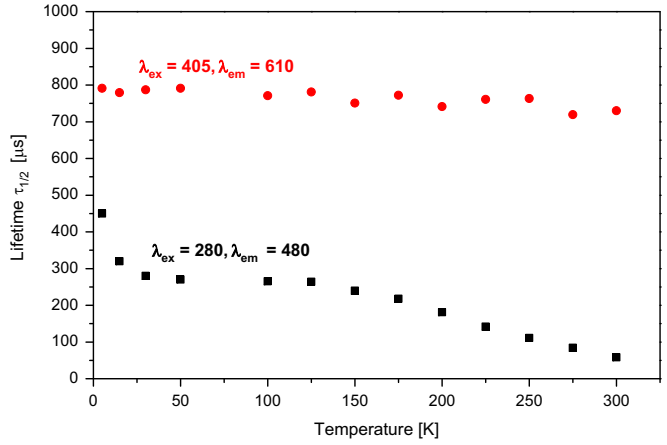


**Fig. 6.** Temperature dependence of lifetime values for the niobate group and the $^4G_{5/2}$ level.

region from samarium ions results in white light luminescence, a feature promising for application in commercial lightning.

Detailed analysis of absorption as well as emission spectra leads to the conclusion that the investigated system may be of interest for the design of visible lasers optically pumped by InGaN/GaN diode lasers. Width of an absorption band at ca. 404 nm that can be used to optically pump the material is insignificantly influenced by temperature, contrary to widths of emission lines. This feature is favorable for the design of cryogenic lasers operating at liquid nitrogen temperature. Laser action at ca. 610 and 656 nm, related to the $^4G_{5/2}$–$^6H_{7/2}$ and $^4G_{5/2}$–$^6H_{9/2}$ transitions, should be possible due to similar $\sigma_{em}$ coefficients.

## Acknowledgments

This work was supported by the National Center of Science of Poland under Grant agreement no 2011/01/N/ST5/05612.

Experiment performed at the Superlumi Station at HASYLAB was supported by the European Community – Research Infrastructure Action under the FP6 "Structuring the European Research Area" Program (through the Integrated Infrastructure Initiative "Integrating Activity on Synchrotron and Free Electron Laser Science") Contract II – 20100281 EC.

## References

[1] A.A. Ballman, S.P.S. Porto, A. Yariv, J. Appl. Phys. 34 (1963) 3155.
[2] Y. Cheng, X. Xu, J. Xu, C. Zhao, X. Yang, X. Liang, S. Zhou, IEEE J. Quantum Electron. 45 (2009) 1571.
[3] A.A. Kaminskii, J. Dong, H.J. Eichler, J. Hanuza, K. Ueda, M. Mączka, H. Rhee, M. Betinelli, Laser Phys. Lett. 6 (2009) 821.
[4] A.A. Kaminskii, J. Dong, K. Ueda, M. Betinelli, M. Grinberg, D. Jaque, Laser Phys. Lett. 6 (2009) 782.
[5] A.H. Buth, G. Blasse, Phys. Status Solidi A 64 (1981) 669.
[6] D. Van der Voort, J.M.E. de Ruk, G. Blasse, Phys. Status Solidi A 135 (1993) 621.
[7] J. Di, X. Xu, C. Xia, H. Zeng, Y. Cheng, D. Li, D. Zhou, F. Wu, J. Cheng, J. Xu, J. Alloys Compd. 536 (2012) 20.
[8] G. Zimmerer, Radiat. Meas. 42 (2007) 859.
[9] J.P. Cummings, S.H. Simonsen, Am. Mineral. 55 (1970) 90.
[10] L. Macalik, M. Mączka, J. Hanuza, P. Godlewska, P. Solarz, W. Ryba-Romanowski, A.A. Kaminskii, J. Alloys Compd. 451 (2008) 232.
[11] R.D. Shanon, Acta Crystallogr. A 32 (1976) 751.
[12] J. Cao, Y. Ji, J. Li, Z. Zhu, Y. Wang, Z. You, C. Tu, J. Lumin. 131 (2011) 1350.
[13] C.K. Jayasankar, E. Rukmini, Opt. Mater. 8 (1997) 193.
[14] B.R. Judd, Phys. Rev. 127 (1962) 750.
[15] G.S. Ofelt, J. Chem. Phys. 37 (1962) 511.
[16] M.P. Hehlen, M.G. Brik, K.W. Kramer, J. Lumin. 136 (2013) 221, http://dx.doi.org/10.1016/j.jlumin.2012.10.035.
[17] L. Srinivasa Rao, M. Srinivasa Reddy, M.V. Ramana Reddy, N. Veeraiah, Physica B 403 (2008) 2542, http://dx.doi.org/10.1016/j.physb.2008.01.043.
[18] R. Praveena, V. Venkatramu, P. Babu, C.K. Jayasankar, Physica B 403 (2008) 3527, http://dx.doi.org/10.1016/j.physb.2008.05.027.
[19] G. Dominak-Dzik, J. Alloys Compd. 391 (2005) 26, http://dx.doi.org/10.1016/j.jallcom.2004.11.014.
[20] M. Sobczyk, D. Szymański, J. Lumin. 142 (2012) 96, http://dx.doi.org/10.1016/j.jlumin.2013.03.062.
[21] G.Q. Wang, Y.F. Lin, X.H. Gong, Y.J. Chen, J.H. Huang, Z.D. Luo, Y.D. Huang, J. Lumin. 147 (2014) 23, http://dx.doi.org/10.1016/j.jlumin.2013.10.058.
[22] P. Van Do, V. Phi Tuyen, V. Xuan Quang, N. Trong Thanh, V. Thi Thai Ha, N.M. Khaidukov, Y.-I. Lee, B.T. Huy, J. Alloys Compd. 520 (2012) 262–265, http://dx.doi.org/10.1016/j.jallcom.2012.01.037.
[23] P. Solarz, R. Ryba-Romanowski, Phys. Rev. B 72 (2005) 075105, http://dx.doi.org/10.1103/PhysRevB.72.075105.
[24] A. Strzep, R. Lisiecki, P. Solarz, G. Dominiak-Dzik, W. Ryba-Romanowski, M. Berkowski, Appl. Phys. B 106 (2012) 85, http://dx.doi.org/10.1007/s00340-011-4731-9.
[25] A. Strzep, R. Lisiecki, P. Solarz, W. Ryba-Romanowski, M. Berkowski, Opt. Mater. 36 (2014) 740, http://dx.doi.org/10.1016/j.optmat.2013.10.040.
[26] C.K. Jayasankar, P. Babu, J. Alloys Compd. 307 (2000) 82.